SIMULTANEOUS GREEN SEPARATION/PRECONCENTRATION AND DETERMINATION OF LEAD IONS IN WATER SAMPLES VIA GRAPHITE FURNACE ATOMIC ABSORPTION SPECTROMETRY**

Rosa Kalantari, Ali Moghimi*, Fariborz Azizinezhad

Department of Chemistry, Varamin Pishva Branch, Islamic Azad University, Varamin, Iran; e-mail: alimoghimi@iauvaramin.ac.ir, kamran9537@yahoo.com, Ali.Moghimi@iaups.ac.ir

A chitosan-functionalized magnetic graphene oxide composite was used to preconcentrate, separate, and determine the trace amounts of lead ions (Pb^{2+}) in aqueous samples. Graphite furnace atomic absorption spectrometry was applied to determine Pb^{2+} concentration in aqueous solutions. Sodium diethyldithiocarbamate was applied as a chelating agent in this study. Fourier transform infrared spectra, X-ray diffraction, thermogravimetric analysis, vibrating sample magnetometer, and scanning electron microscope were applied to characterize the magnetic properties, surface morphology, and chemical structure of the synthesized composite. Factors that affected extraction efficiency were evaluated and optimized. Under optimal conditions, the linearity limit for the determination of Pb^{2+} ion concentration was 0.70–100.00 μg/L with a correlation coefficient of 0.9981. The quantitation and detection limits were 0.73 and 0.21 μg/L, respectively. The value of the preconcentration factor was found to be 40, and the repeatability coefficient of the proposed method was calculated as 2.58% (RSD%). Further, the isothermal models, kinetic data, and thermodynamic studies were investigated. Overall, the proposed method is an effective technique with many advantages such as high sensitivity, economical procedure, fast and easy separation ability with excellent recovery, and being environmentally friendly to determine trace amounts of Pb^{2+} ions in various aqueous samples.

Keywords: *magnetic separation, biosorbent, lead ions, water samples, adsorption, Graphite furnace atomic absorption spectrometry*.

ОДНОВРЕМЕННОЕ РАЗДЕЛЕНИЕ/ПРЕКОНЦЕНТРИРОВАНИЕ И ОПРЕДЕЛЕНИЕ ИОНОВ СВИНЦА В ПРОБАХ ВОДЫ МЕТОДОМ АТОМНО-АБСОРБЦИОННОЙ СПЕКТРОМЕТРИИ В ГРАФИТОВОЙ ПЕЧИ

R. Kalantari, A. Moghimi*, F. Azizinezhad

УДК 543.42:546.815/.819

Исламский университет Азад, Варамин, Иран; e-mail: alimoghimi@iauvaramin.ac.ir, kamran9537@yahoo.com, Ali.Moghimi@iaups.ac.ir

(Поступила 30 мая 2022)

Композит магнитного оксида графена, функционализированный хитозаном, использован для предварительного концентрирования, разделения и определения следовых количеств ионов свинца (Pb^{2+}) в водных образцах. Концентрация Pb^{2+} в водных растворах определена с помощью атомно-абсорбционной спектрометрии с графитовой печью. В качестве хелатирующего агента применен диэтилдитиокарбамат натрия. ИК-Фурье-спектроскопия, рентгеновская дифракция, термогравиметрический анализ, вибрационная магнитометрия и сканирующая электронная микроскопия использованы для характеристики магнитных свойств, морфологии поверхности и химической структуры синтезированного композита. Оценены и оптимизированы факторы, влияющие на эффективность извлечения. В оптимальных условиях предел линейности определения концентрации ионов Pb^{2+} 0.70–100.00 мкг/л с коэффициентом корреляции 0.9981, пределы количественного определения

** Full text is published in JAS V. 90, No. 3 (http://springer.com/journal/10812) and in electronic version of ZhPS V. 90, No. 3 (http://www.elibrary.ru/title_about.asp?id=7318; sales@elibrary.ru).

и обнаружения 0.73 и 0.21 мкг/л, коэффициент концентрирования 40, коэффициент повторяемости метода 2.58 % (RSD%). Изучены изотермические модели, проведены термодинамические исследования. Предлагаемый метод эффективен и обладает высокой чувствительностью, экономичностью, возможностью быстрого и легкого разделения, а также экологичностью при определении следовых количеств ионов Pb^{2+} в различных водных образцах.

Ключевые слова: *магнитная сепарация, биосорбент, ионы свинца, пробы воды, адсорбция, атомно-абсорбционная спектрометрия с графитовой печью.*

Introduction. The disposal of various industrial and domestic effluents into the environment and the infiltration of these substances deep into the soil cause soil and groundwater pollution. To solve this problem, researchers have always been trying to find new methods to remove pollutants from the environment. Heavy metals, especially lead (Pb), are pollutants that cause serious diseases in humans even in small amounts [1, 2]. Nowadays, various technologies are applied to remove heavy metals from aqueous solutions such as ion extraction, reverse osmosis, ion exchange, chemical precipitation, and ion adsorption. Recently, the application of the adsorption method has attracted much attention as it offers significant advantages such as simplicity, low cost, insensitivity to toxic substances, and effective removal of metal ions from aqueous solutions [3]. Heavy metals cannot be determined directly due to complex matrices in the environment. Magnetic nanoparticles have particular advantages including specific physicochemical properties, high surface-to-volume ratio, reduced generation of secondary waste, easy separation due to their magnetic properties, and easy recovery of the adsorbent [4].

Today, the use of carbon structures and polymers in industry as well as the manufacture of various compounds to remove pollutants, drug delivery, and flame retardants is very significant. Graphene oxide (GO) exhibits many important properties, including being light in weight, having a large cross-section, nontoxicity, high chemical and thermal stability, higher porosity, higher adsorption capacity, and lower cost. The presence of COOH and OH groups in GO facilitates coordination with metal ions [5–7]. To enhance the effectiveness of GO sheets as adsorbents for heavy metals, their surface is usually chemically or physically modified and functionalized before use. The presence of chemical groups on the GO surface prevents the accumulation as well as agglomeration of these particles and helps them disperse better in the polymer [8]. Chitosan (CS) is used as an adsorbent for the removal of heavy metals due to its high hydrophilic properties with amino and hydroxyl groups, as well as its flexible structure. Other important characteristics of CS include its biocompatibility and nontoxicity [9]. Dispersive solid-phase extraction (DSPE) is a sample preparation method for analysis. In this technique, the adsorbent is completely dispersed in the sample solution by increasing the interaction between the sample and the adsorbent as well as adsorbing the sample on the adsorbent surface. Finally, the analyte is eluted from the adsorbent with a solvent and determined further [10].

In this study, magnetic GO (mGO) sheets were functionalized with CS, thereby generating an adsorbent capable of adsorbing lead ions (Pb^{2+}) from aqueous samples. The synthesized magnetic composite (magnetic graphene oxide–chitosan (mGO–CS)) was analyzed by Fourier transform infrared (FTIR) spectroscopy, X-ray diffraction (XRD), thermogravimetric analysis (TGA), scanning electron microscopy (SEM), and vibrating sample magnetometry (VSM) methods. Then, the effective and important parameters in the extraction of Pb^{2+} ions were studied and optimized. Finally, the removal of Pb^{2+} ions in various aqueous samples was studied to evaluate the applicability of the proposed technique.

Experimental. Graphite flakes (6–10 microns) (99.0%) and CS with 80 mesh, a deacetylation degree of 96% and an average molecular weight of 6.35×10^5 were prepared by Sigma-Aldrich. $FeCl_2 \cdot 4H_2O$ and $FeCl_3 \cdot 6H_2O$ were purchased from Merck (Darmstadt Germany). The reagents 1-ethyl-3-(3-dimethylaminopropyl) carbodiimide hydrochloride (EDC), N-hydroxylsuccinimide (NHS), and sodium diethyldithiocarbamate (DDTC) were purchased from Aldrich Products. The stock of Pb^{2+} solutions (1000 mg/L) was obtained by dissolving $Pb(NO_3)_2$ in deionized (DI) water. All chemicals used in the current study were of analytical grade, and DI water was applied for all tests.

A graphite furnace atomic absorption spectrometer (GF–AAS) was utilized to determine the Pb^{2+} concentration in the samples (Agilent, model 240 AA, USA), and a Pb hollow cathode lamp was employed as the radiation source. The FTIR spectrometer (Perkin Elmer, USA) was used at 4000–400 cm^{-1} with the standard KBr disk technique. Thermogravimetric analysis was performed using Bahr STA-503 (Germany). A Philips PW 12C diffractometer (Philips PW, Amsterdam, The Netherlands) was employed to record the XRD powder patterns by CuK_α-radiation. The SEM images were acquired via SEM (PHILIPS, CM120, Amsterdam, The Netherlands). Magnetization measurements were performed using an AGFM/VSM3886 VSM

(Meghnatis Daghigh Kavir Company, Iran). A super magnet with a 1.4 T magnetic field (N35 model from Tehran Magnet, Tehran, Iran) was utilized to achieve magnetic separation.

The GO was prepared through the oxidation of graphene powder according to the Hummers method [11, 12]. First, 150 mg of the synthesized GO was placed in a flask with 25 mL of DI water and then placed in an ultrasonic bath at 50°C for 2 h to disperse and homogenize it completely. Next, a solution of 0.540 g ferric chloride ($FeCl_3 \cdot 6H_2O$, 2 mmol) and 0.198 g ferrous chloride ($FeCl_2 \cdot 4H_2O$, 4 mmol) was prepared by dissolving in 25 mL DI water, which was gradually added to the GO solution with constant stirring. The obtained solution was kept in a water bath at 60°C for 30 min with automatic stirring. Once the black mixture was cooled down, 80 mL of a 1.25 mol/L NH_3 solution was added dropwise. Then the mixture was kept at 60°C for 30 min under continuous automatic stirring in a water bath and degassed through nitrogen purging to prevent the entry of oxygen. The solution was rinsed five times with DI water, and the precipitate was separated from the solution by an external magnetic field with 1.4 T power. Finally, the obtained precipitate was dried at 50°C for 5 h in a vacuum oven [12].

For synthesis of mGO–CS nanocomposite 1 g of CS powder was completely dissolved in 30 mL of 3% CH_3COOH to prepare a 4 mg/L CS solution. Then, 0.1 g of mGO was dispersed in 25 mL of DI water under an ultrasonic bath for 15 min. To activate the carboxyl groups of GO, 0.5 mL of a 0.05 mol/L EDC solution and 0.5 mL of a 0.05 mol/L NHS solution were added. The resulting solution was mixed with 25 mL of a 4 mg/L CS solution, dispersed, and homogenized under ultrasonication for 15 min. The mixture was then kept in a water bath at 50°C for 3 h. At this stage, CS reacts with mGO, where the amine groups of CS interact with the carboxyl groups of GO, resulting in the NH_2-grafted mGO composite. The resulting precipitate was separated from the solution using an external magnetic field (1.4 T) and dried in a vacuum oven at 50°C for 5 h (Fig. 1).

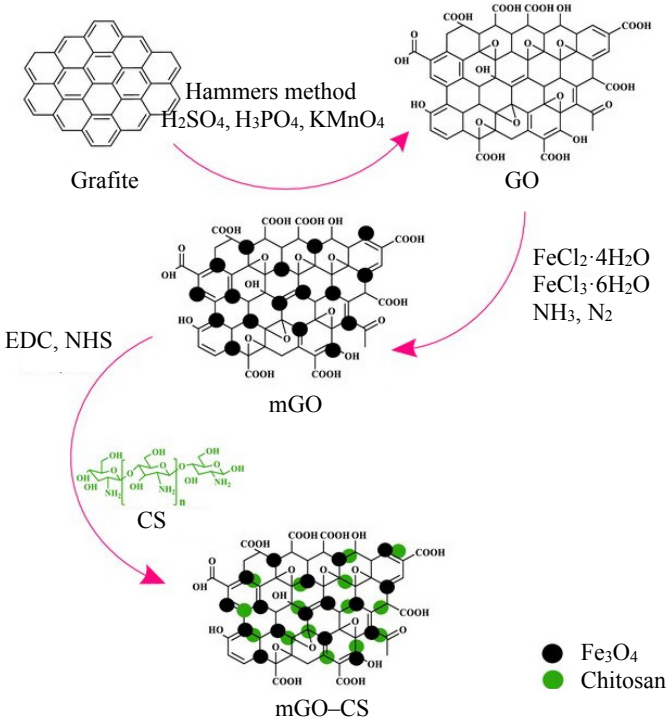

Fig. 1. Schematic representation of the method for the mGO–CS nanocomposite preparation.

For adsorption experiments first, 200 mL of a 50 µg/L Pb^{2+} ion solution and 0.5 mL of 12 µg/mL DDTC solution were added to a flask. The mixture was stirred for 15 min until the complexation reaction took place. The reaction is as follows [13]:

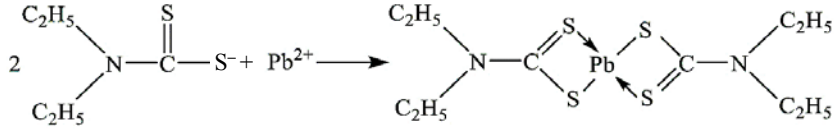

Then, the pH was adjusted to 6.0 with 2 mL of acetate buffer solution. Next, 90 mg of the presynthesized adsorbent was added 2.0 mL of the buffer solution, acetic acid/acetate 1.0 mol/L, was used to adjust the desired pH. To carry out the equilibrium reaction, the flask was shaken at 150 rpm for 20 min. After the equilibrium time, when the adsorption process was completed, the adsorbent was separated from the solution using an external magnetic field. For separating the residual concentration of the Pb^{2+} ion in the solution, the magnet was used for separation from the mGO–CS adsorbent. Then, 5 mL of a 3 mol/L HNO_3 solution was added to the adsorbent as a suitable eluent and homogenized by shaking for 5 min. Finally, the adsorbent was re-isolated from the solution using an external magnetic field. The analyte concentration was determined in the aqueous phase using the GF–AAS. The number of metal ions removed by the adsorbent was calculated using q_e (the adsorption capacity of metal ions on adsorbents; μg/g):

$$q_e = \frac{(C_0 - C_e)V}{m}, \quad (1)$$

where C_0 (μg/L) is the initial concentration of the metal ion, C_e (μg/L) is the equilibrium concentration of the metal ion, V (L) is the volume of the ion solutions, and m (g/L) is the dry weight of the adsorbent. The removal efficiency of each ion was calculated using:

$$R = \frac{(C_0 - C_e)}{C_0} \times 100\%, \quad (2)$$

where R is the removal efficiency of each ion from the solution, C_0 is the initial concentration, and C_e (μg/L) is the final concentration after the completion of the bonding time with the adsorbent.

Regarding the procedure, 0.09 g of adsorbent was used to estimate the pHzpc of the mGO–CS adsorbent. Further, 20 mL of 0.1 mol/L sodium chloride was prepared to which 0.09 g of mGO–CS adsorbent was added. The pH values were adjusted within 2.0–10.0. For 24 h, the solutions containing the adsorbent were stirred. Next. the pH was measured. The difference between the initial and final pH readings was used to determine the ΔpH value ($\Delta pH = pH_i - pH_f$), and a plot of ΔpH vs pH_i was drawn.

Results and discussion. *Infrared spectra analysis.* The results of FTIR analysis of GO are illustrated in Fig. 2a. In the FTIR spectra, the peaks at 3443, 2923, 1629, 1401, 1207, and 1055 cm^{-1} corresponded to the nano-GO. The peaks at 1055 and 1629 cm^{-1} corresponded to C–O bond and C=O stretching bond, respectively. Also, the peaks at 2923 and 3443 cm^{-1} matched the symmetric C–H stretching vibration and stretching vibration of –OH in GO, respectively. Further, the peak at 1401 cm^{-1} belonged to C–OH stretching vibration. The spectra at 1207 and 1055 cm^{-1} represented the epoxy and alkoxy functional groups in GO [14]. The peak identified at 695 cm^{-1} was associated with the bending vibration of the Fe–O band in Fe_3O_4 (Fig. 2a, mGO), representing the magnetic properties of GO [14, 15]. In Fig. 2a mGO–CS spectra, the peak at 1562 cm^{-1} belongs the N–H groups, which represents the amidation reaction between the carboxyl groups on GO and the amine groups of CS. In addition, the functional groups OH and NH_2 overlapped and produced a broad peak at 3457 cm^{-1}. This broad peak was related to the vibration of the functional groups $–NH_2$ and –OH of CS with oxygen-containing functional groups of GO (epoxy and alkoxy). Furthermore, the newly appeared peaks at 1479 and 1562 cm^{-1} corresponded to $–CH_2$ and –CONH groups. The peaks generated by mGO–CS within the range of 1295 and 1132 cm^{-1} was related to the tensile vibrations of C–N and NH_2 groups, respectively [16].

X-ray diffraction analysis. According to the obtained spectra (Fig. 2b, GO), the diffraction peak at 2θ = 10.42° explained the graphite oxide structure caused by the oxidation of the graphene plane. According to the XRD pattern of graphite, the diffraction peak for graphene appeared at 2θ=26.45° [17]. In Figure 2b mGO, peaks at 2θ = 25.22, 32.55, 41.16, 54.48, 58.43, and 66.04° correspond to (220), (311), (400), (422), (511), and (440), respectively, confirming the presence of Fe_3O_4 particles [17, 18]. The weak peak at 2θ = 27.33° in mGO–CS could be attributed to the amidation reaction between the carboxyl groups on GO and amine groups of CS [18].

Scanning electron microscopy images. The SEM results (Fig. 3a) indicated that the GO synthesized by the Hummer method had a sheet-like structure with a wrinkled edge and smooth surface. The spectra of SEM in Fig. 3b mGO reveal that the GO sheets are coated with Fe_3O_4 particles with a polygonal and spherical shape, confirming the modified GO magnetic properties. As displayed in Fig. 3c mGO–CS, the surface porosity is occupied by CS. Indeed, the functional carboxyl groups of the GO structure were connected to the functional amine groups of the CS structure [16, 18].

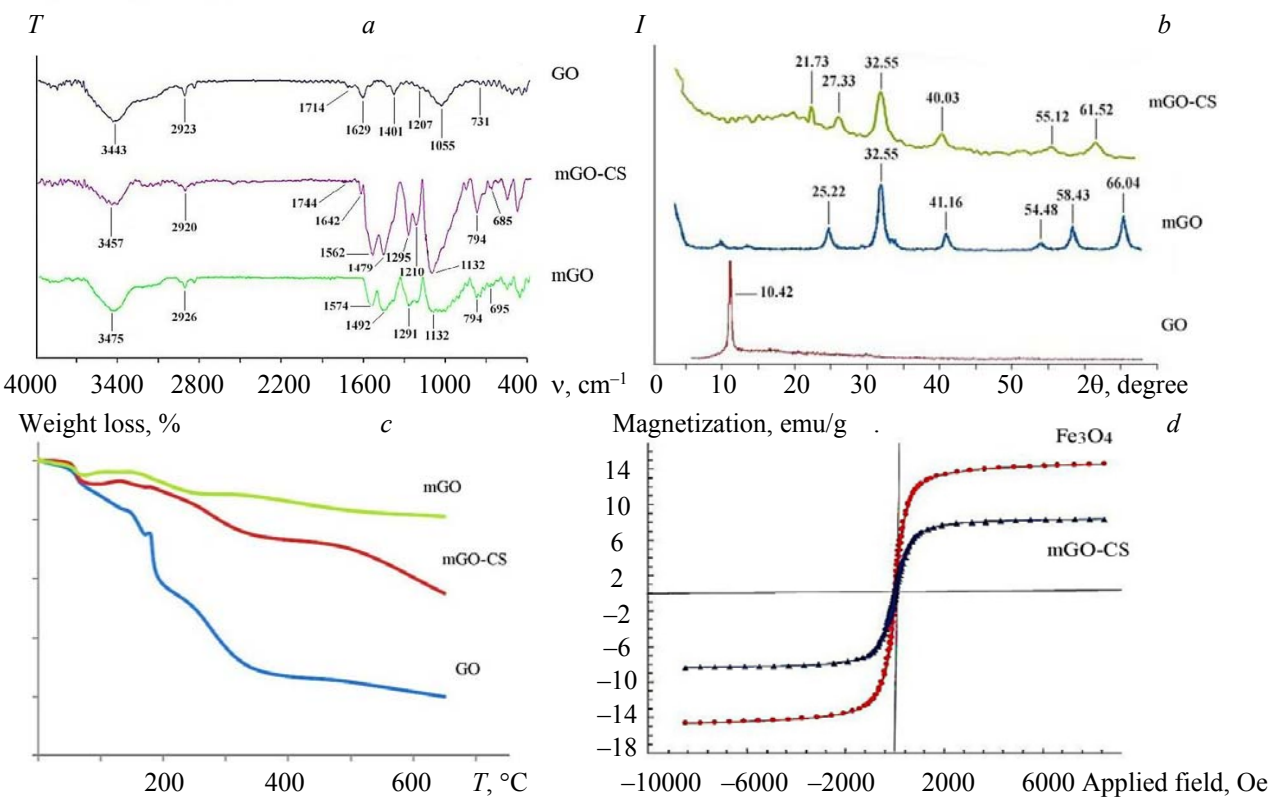

Fig. 2. Characterization of the adsorbent: (a) FTIR spectra of GO, mGO, mGO–CS, (b) XRD patterns of GO, mGO, mGO–CS, (c) TGA analysis of GO, mGO, mGO–CS, and (d) VSM magnetization curves of Fe_3O_4 and mGO–CS at room temperature.

Thermogravimetric analysis. In the curves of mGO–CS and GO (Fig. 2c), the first step of weight loss of the magnetic nanocomposite occurred at a temperature below 100°C, which is related to the evaporation of residual moisture in the composite structure. The second weight loss, about 10%, was observed at 160–250°C and was due to the degradation of the functional groups of GO, which was observed at lower temperatures compared to pure GO. In this step, the formation of the strong covalent bond between GO and CS was responsible for the weight loss of the composite compared to pure GO. The third weight loss occurred at 470°C, related to the degradation of CS [19].

Vibrating sample magnetometry analysis. The adsorbent mGO–CS was placed under a magnetic field. As represented in Fig. 2d and the magnetization curve, the magnetic values of the Fe_3O_4 nanoparticles and magnetic nanocomposite mGO–CS at room temperature are 15 and 8 emu/g, respectively. The obvious reduction from 15 to 8 emu/g was due to the formation of strong chemical bonds between the functional groups of GO plus CS and the Fe_3O_4 particles [15, 19].

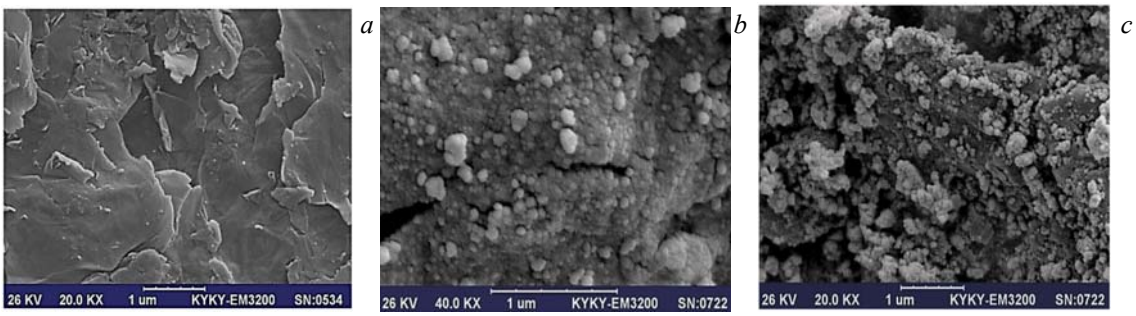

Fig. 3. (a) SEM image of GO, (b) SEM image of mGO, (c) SEM image of mGO–CS.

Optimization of adsorption conditions. pH has a key role in the metal–DDTC chelate formation and its subsequent extraction. The effect of pH on the recovery of Pb^{2+} ions was evaluated at pH 2.0–10.0. As depicted in Fig. 4a, the extraction recovery has diminished at pH > 6 due to metals' precipitation as hydroxides. The chelating agent at pH < 6 was protonated and the recovery was reduced. The H^+ ions bind to amine functional groups on the adsorbent surface when the pH is low; thus, at pH 6, an excellent complexation coefficient was achieved between the Pb^{2+} ions and DDTC [4, 20]. A pH value ΔpH of zero was used to determine the point of zero charge (pHzpc). The ZPC point is the point at which ΔpH is zero. The pH values at which there are equal amounts of acidic and basic functional groups are known as the zero charges of solid surfaces. ΔpH vs pH_i is indicated in Fig. 4b. This value for the adsorbent mGO–CS was found to be about 5.6, suggesting that acidic groups predominate on the surface of an mGO–CS adsorbent. According to Fig. 4b, at pH_i < 5.6, when ΔpH > 0, the adsorbent was protonated and its surface was positively charged. On the other hand, at pH_i values >5.6, when ΔpH < 0, the adsorbent was deprotonated and its surface was negatively charged [21].

To estimate the optimum amount of the adsorbent, various amounts of it were studied within the range of 5–150 mg/L. As displayed in Fig. 4c, the optimum value has been 90 mg/L, where the percentage adsorption value and recovery value were maximum. Thus, increasing the absorbent content enhances the surface sites available for ion adsorption, which boosts the adsorption efficiency. However, with a lower adsorbent dosage, the active sites accessible for ion adsorption are quickly saturated, resulting in a significant decline in the adsorption efficiency [4, 22].

The recovery of Pb^{2+} ions was investigated at time intervals of 1–25 min. As shown in Fig. 4d, the ion adsorption efficiency increased with reaction time, with the Pb^{2+} ion extraction after the reaction of 20 min, which means that after 20 min, the equilibrium between Pb^{2+} ions and adsorption was reached, and the adsorption process was finished. Thus, a high adsorption rate was observed at the beginning of the adsorption process, owing to the presence of voids that can trap Pb^{2+} ions. However, over time, the efficiency diminished due to the saturation of the sites on the adsorbent surface [4, 21].

The type of solvent that can be leached out has also a great effect on enhancing the recovery and adsorption efficiencies which thus should be carefully selected. According to the results obtained (Fig. 4e), all acidic eluents had reasonable elution ability for the recovery of Pb^{2+} ions; however, HNO_3 solution demonstrated the maximum elution recovery for Pb^{2+} ions. The acidic media could dissolve the probable precipitates and enhance the recovery efficiency of Pb^{2+} ions; thus, 3 mol/L HNO_3 was found to be an excellent eluent for the other adsorption processes as well [22].

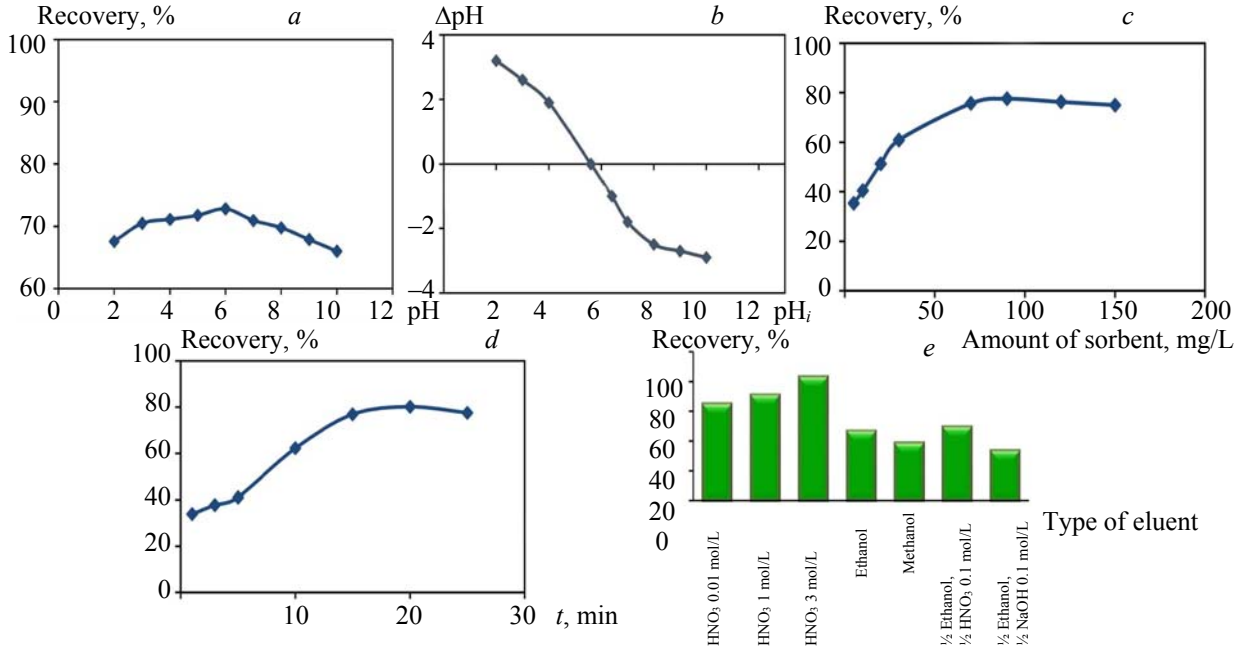

Fig. 4. (a) Influence of pH, (b) zero charge, (c) adsorbent amount, (d) contact time, (e) eluent type on Pb^{2+} adsorption on mGO–CS (n = 3). Experimental parameters: C_0 (Pb^{2+}) = 50 μg/L, C(DDTC) = 12 μg/mL, sample volume = 200 mL, pH in c, d, e = 6.0, adsorbent dose = 90 mg/L in a, b, d, e, contact time = 20 min in a, c, e, eluent type = 3 mol/L HNO_3 in a, c, d, and T = 25°C.

An ion is an interfering ion if it causes a change of > ±5% in the adsorption and recovery of Pb^{2+} ions. The adsorption process was carried out under the determined optimal conditions using 200 mL of a 50 μg/L Pb^{2+} solution plus DDTC as a chelating agent in the presence of various concentrations of the interfering ions. Then, the adsorption of the recovered solution was measured and compared with that of the solution obtained when the sample was recovered without interfering ions. According to Table 1, the Pb^{2+} ion has been recovered in the presence of foreign ions with a deviation of ±5% and, at the same time, the foreign ions have had no significant effect and interference on the measurement [23, 24].

TABLE 1. Effect of Foreign Ions on the Percentage Recovery of 50 μg/L Pb^{2+} in Water Samples (n = 3)

Diverse ion	Concentration, μg/L	Recovery*, %
Na^+	5000	98.12 ± 2.82
K^+	5000	93.04 ± 1.65
Mg^{2+}	100	94.47 ± 1.91
Zn^{2+}	5	97.61 ± 2.34
Ni^{2+}	5	94.07 ± 1.86
CO_3^{2-}	1500	98.12 ± 1.33
Ag^+	5	96.05 ± 2.14
Cd^{2+}	5	98.92 ± 1.13
SO_4^{2-}	1000	95.87 ± 2.58
Cl^-	5000	93.40 ± 2.43
Ca^{2+}	1000	93.42 ± 2.16
Mn^{2+}	5	91.83 ± 1.97

*Mean ± standard deviation.

To better understand the adsorption mechanism of the adsorbed ion on the surface of the adsorbent, the obtained data were analyzed using isothermal models. In this study, Freundlich and Langmuir isothermal models were utilized. The Langmuir model is based on the homogeneous and monolayer adsorption of metal ions with equivalent energy over the entire adsorbent surface using [25, 26]:

$$C_e / q_e = 1 / k_L q_{\max} + C_e / q_{\max}, \quad (3)$$

where q_e is the adsorption capacity of metal ions on adsorbents (μg/g), C_e (μg/L) denotes the metal ion concentration at equilibrium, K_L (L/μg) is the Langmuir constant corresponding to the binding energy of adsorption, and $q_{\max}$ (μg/g) reflects the maximum capacity of ion uptake on the adsorbent. In contrast, according to Eq. (4), the Freundlich model is based on the multilayer and heterogeneous adsorption processes:

$$\ln q_e = \ln K_F + 1 / n\left(\ln C_e\right), \quad (4)$$

where K_F and n are the Freundlich isothermal constants, where K_F (μg/g)(μg/L)$^{-n}$ is the adsorption capacity and n refers to the adsorption force. According to the R^2 values summarized in Fig. 5, the adsorption isotherm follows the Freundlich model with a high R^2 value, indicating that the adsorption of Pb^{2+} ions on the adsorbent surface is multilayer. Further, the $q_{\max}$ for Pb^{2+} ions was found to be 120.48 μg/g [21]. Langmuir and Freundlich model parameters for the Pb^{2+} ions adsorption onto mGO–CS are: K_L = 0.0037 L/μg, R^2 = 0.9406; n = 1.47, K_F = 1.34 (μg/g)(μg/L)$^{-n}$, R^2 = 0.9921.

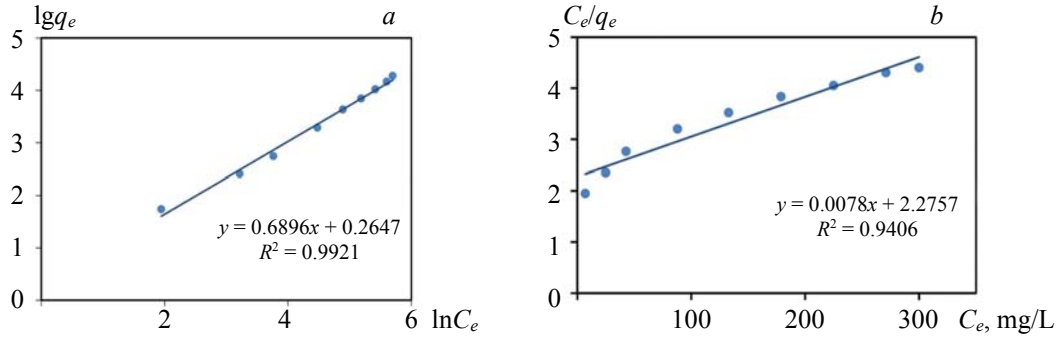

Fig. 5. (a) Freundlich and (b) Langmuir isothermal models for the adsorption of Pb^{2+}.

The removal process of Pb^{2+} ions via pseudo-first- and second-order kinetic models was investigated and validated using the obtained R^2. The pseudo-first-order kinetic model is explained:

$$1/q_t = k_1/q_e t + 1/q_e, \quad (5)$$

where q_t (μg/g) is the adsorbed number of metal ions on the adsorbent at time t (min), k_1 represents the pseudo-first-order rate constant for the kinetic model (min^{-1}), and q_e (μg/g) shows the adsorbed number of metal ions on the synthesized adsorbent at equilibrium. The pseudo-second-order kinetic model is calculated based on

$$t/q_t = 1/k_2 q_e^2 + t/q_e, \quad (6)$$

where k_2 (g/μg min) denotes the pseudo-second-order rate constant of adsorption. According to Fig. 6, and the obtained R^2 values, the removal process of Pb^{2+} ions agrees better with the pseudo-second-order kinetic model since the R^2 values are higher. In the adsorption process, chemical adsorption is the rate-limiting step [21, 27]. Estimated adsorption kinetic parameters for adsorption of Pb^{2+} on mGO–CS: $q_e = 38.46$ μg/g, $K_1 = 0.5653$ min^{-1}, $R^2 = 0.9660$ for pseudo-first-order model; $q_e = 39.37$ μg/g, $K_2 = 0.0435$ g/mg · min, $R^2 = 0.9986$ for pseudo-second-order model.

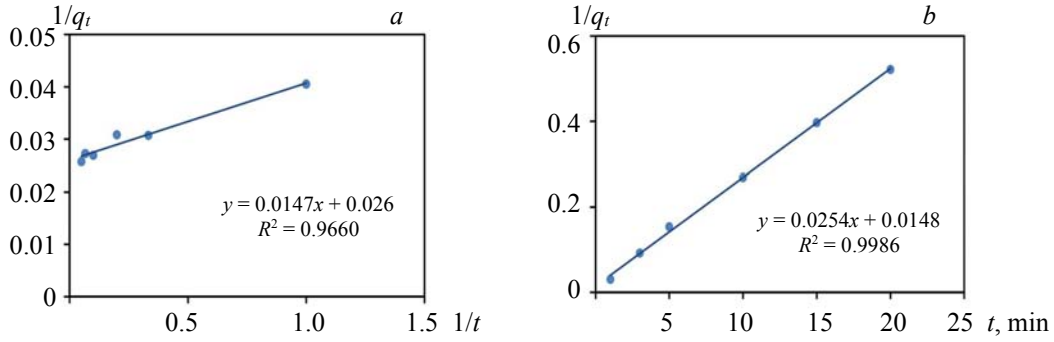

Fig. 6. (a) Pseudo-first-order and (b) Pseudo-second-order kinetics for the uptake of Pb^{2+} on mGO–CS.

Thermodynamic parameters are very important and depend on the adsorption process. The thermodynamic data such as $\Delta H°$, $\Delta G°$, and $\Delta S°$ in the adsorption behavior can be calculated:

$$\ln K_d = \Delta S°/R - \Delta H°/RT, \quad (7)$$

$$\Delta G° = -RT \ln K_d, \quad (8)$$

$$\Delta G° = \Delta H° - T\Delta S°, \quad (9)$$

where $\Delta H°$ (KJ/mol) is the standard enthalpy change, $\Delta S°$ (kJ/mol K) is standard entropy change, $\Delta G°$ (kJ/mol) is the standard Gibbs free energy change, K_d (L/g) is the adsorption equilibrium constant, T (K) is the temperature, and R (8.314 J/mol K) is the universal gas constant. All thermodynamic data are listed in Table 2. According to the obtained data, the positive $\Delta H°$ values and the negative $\Delta G°$ values indicated that the adsorption process was spontaneous and endothermic. The positive $\Delta S°$ values revealed that the irregularity of Pb^{2+} ions increased along the adsorption [27]. All analytical figures were obtained based on the calibration curves for ten different concentrations (calibration equation $y = 0.0075x - 0.0126$; $R^2 = 0.9981$, LOD = 0.21 μg/L, LOQ = 0.73 μg/L, PF = 40, RSD (%) (50 μg/L) = 2.58 and 2.36 for intra- and inter-day).

The regenerability of the synthetic adsorbent after applying the desorption-adsorption cycle is an economically important and cost-effective necessity. To evaluate the possibility of reusing the adsorbent, this section reports on the conducted adsorption-desorption tests of Pb^{2+} ions via the adsorbent under optimal conditions in five consecutive cycles (Fig. 7). In the first four cycles, the adsorption percentage remained constant at 90%; however, in the fifth cycle, the removal efficiency of Pb^{2+} ions diminished to less than 90%. Thus, the synthesized adsorbent mGO–CS can be reused up to four times, and it can be effectively used to remove Pb^{2+} ions from the aqueous solution [1, 21].

TABLE 2. Thermodynamic Parameter Data for the Adsorption of Pb^{2+}on mGO–CS

T, K	K_d, L/g	$\Delta G°$, kJ/mol	$\Delta S°$, kJ/mol K	$\Delta H°$, kJ/mol	R^2
288	2.73	–1.45	0.12	34.25	0.9991
298	4.02	–2.69			
308	6.29	–3.93			
318	9.37	–5.17			

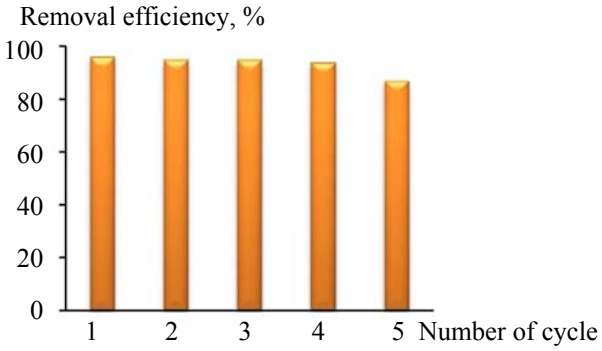

Fig. 7. Reusability of mGO–CS.

To investigate the applicability of the proposed method for determining Pb^{2+} ions in real samples, the concentration of Pb^{2+} ions was measured in several different aqueous and biological samples with a volume of 200 mL. In this regard, the concentration of various solution samples was determined. These samples included tap water (taken after running the tap for 15 min, Tehran, January 12, 2022), seawater (taken from Caspian Sea, January 17, 2022), well water (Varamin, February 8, 2022), and wastewater (taken from industrial wastewater of Iran Khodro, February 12, 2022) (Table 3).

TABLE 3. Determination of Pb^{2+} in Real Water Samples (n = 3)

Sample	Spiked, μg/L	Found, Mean ± standard deviation, μg/L	Relative recovery, %
Tap water	0.0	ND	
	5.0	4.82 ± 1.43	96.40 ± 2.30
	20.0	19.96 ± 2.26	99.80 ± 1.71
Well water	0.0	ND	
	5.0	4.71 ± 1.53	94.21 ± 2.47
	20.0	19.38 ± 2.19	96.92 ± 1.89
Sea water	0.0	1.82 ± 1.27	
	5.0	6.47 ± 1.84	93.00 ± 2.06
	20.0	20.87 ± 2.15	95.25 ± 1.79
Industrial wastewater	0.0	3.94 ± 1.44	
	5.0	8.55 ± 2.36	92.20 ± 2.36
	20.0	21.73 ± 1.67	88.95 ± 1.83

N o t e. ND is not detected.

TABLE 4. Comparison of the Proposed Method with Other Studies

Method	Adsorbent	LOD, μg/L	RSD, %	Sample	Reference
MSPE–FAAS	Fe_3O_4-SiO_2-Bacillus pumilis	4.62	3.60	water	[22]
UA–MSPE–FAAS	SH–GO–Fe_3O_4	14.1	5.04	water	[28]
SPE–FAAS	MWCNT-$MoSe_2$	28.2	7.0	water	[29]
MDSPE–GF–AAS	mGO–CS	0.21	2.58	water	This work

N o t e. MSPE: Magnetic solid phase extraction, FAAS: Flame atomic absorption spectrometry, UA–MSPE: Ultrasonic–assisted magnetic solid phase extraction, SPE: Solid phase extraction, MDSPE: Magnetic dispersive solid phase extraction, GF–AAS: Graphite furnace–atomic absorption spectrometry, SH–GO–Fe_3O_4: Thiol–functionalized graphene oxide–iron oxide, MWCNT: Multiwalled carbon nanotube, GO: Graphene oxide, mGO–CS: Magnetic graphene oxide–chitosan.

As outlined in Table 4, the utilized method has been superior to the other methods due to good repeatability and low LOD. The nano-adsorbent can be isolated within a short time using a magnet without the need for centrifuges and filtrations. Further, the magnetic DSPE (MDSPE) method minimizes the use of toxic and expensive organic solvents.

Conclusions. The surface of magnetic nanoparticles was modified with chitosan to improve the adsorption properties of Graphene oxide and produce the corresponding functional groups to achieve higher efficiency and better absorption of Pb^{2+} ions. Subsequently, the synthesized magnetic nanocomposite (mGO–CS) was used as an effective adsorbent with high efficiency to remove Pb^{2+} ions with DDTC as the chelating reagent from various solutions by Magnetic dispersive solid phase extraction. The q_{max} for Pb^{2+} ions was 120.48 μg/g at pH 6. The application of nanomagnetic adsorbents in the Magnetic dispersive solid phase extraction technique is very important due to their large contact area and high adsorption capacity. Ultimately, the proposed method provides an effective technique with significant features such as high sensitivity, fast separation rate, high adsorption capacity, and good recovery for measuring trace levels of Pb^{2+} ions in various aqueous samples.

Acknowledgements. The current study was supported by Islamic Azad University, Varamin Pishva Branch.

REFERENCES

1. Q. U. Ain, M. U. Farooq, M. I. Jalees, *J. Water Proc. Eng.*, **33**, 101044 (2020).
2. F. Fu, Q. Wang, *J. Environ. Manage*., **92**, 407–418 (2011).
3. A. Moghimi, M. Abniki, *Russ. J. Phys. Chem. B*, **15**, S130–S139 (2021).
4. T. Pourshamsi, F. Amri, M. Abniki, *J. Iran. Chem. Soc.*, **18**, 245–264 (2021).
5. A. Moghimi, M. Abniki, *Chem. Methodologies*, **5**, 250–258 (2021).
6. M. Abniki, Z. Azizi, H. A. Panahi, *IET Nanobiotechnology*, **15**, 664–673 (2021).
7. M. Abniki, A. Moghimi, F. Azizinejad, *J. Serb. Chem. Soc.*, **85**, 1223–1235 (2020).
8. M. Abniki, A. Moghimi, F. Azizinejad, *J. Chin. Chem. Soc.*, **68**, 343–352 (2021).
9. F. Sharifianjazi, A. J. Rad, A. Esmaeilkhanian, F. Niazvand, A. Bakhtiari, L. Bazli, M. Abniki, M. Irani, A. Moghanian, *Biomed. Mater.* (**2021**).
10. S. Büyüktiryaki, R. Keçili, C. M. Hussain, *TrAC, Trends Anal. Chem*., **127**, 115893 (2020).
11. A. Moghimi. M. Abniki, *Adv. J. Chem.Sec. A*, **4**, 78–86 (2021).
12. A. Sharif, M. Khorasani, F. Shemirani, *J. Inorg. Organomet. Polym. Mater*., **28**, 2375–2387 (2018).
13. W. Liu, H. Duan, D. Wei, B. Cui, X. Wang, *J. Mol. Struct.*, **1184**, 375–381 (2019).
14. L. T. M. Thy, N. H. Thuong, T. H. Tu, H. M. Nam, N. H. Hieu, M. T. Phong, *Adv. Nat. Sci.: Nanosci. Nanotechnol*., **10**, 025006 (2019).
15. J. Shen, M. Shi, H. Ma, B. Yan, N. Li, M. Ye, *Mater. Res. Bull*., **46**, 2077–2083 (2011).
16. M. Abniki, A. Moghimi, *Current Anal. Chem.*, **18**, 1–11 (2022).
17. K. Molaei, H. Bagheri, A. A. Asgharinezhad, H. Ebrahimzadeh, M. Shamsipur, *Talanta*, **167**, 607–616 (2017).
18. X. Dong, X. Gao, J. Song, L. Zhao, *Food Chem*., **360**, 130023 (2021).
19. Z. Lu, J. Yu, H. Zeng, Q. Liu, *Sep. Purif. Technol*., **183**, 249–257 (2017).
20. R. Motallebi, A. Moghimi, H. Shahbazi, H. Faraji, *Rev. Roum. Chim*., **65**, 293–305 (2020).
21. N. Salehi, A. Moghimi, H. Shahbazi, *Int. J. Environ. Anal. Chem*., 1–17 (2020).
22. A. Moghimi, M. Abniki, *J. Color Sci. Technol.*, **15**, 301–315 (2022).
23. A. Moghimi, *Russ. J. Phys. Chem. A*, **87**, 1203–1209 (2013).
24. M. S. Arain, T. G. Kazi, H. I. Afridi, M. Bilal, J. Ali, A. Haseeb, *J. Ind. Eng. Chem.*, **62**, 58–63 (2018).
25. A. Moghimi, M. Abniki, M. Khalaj, M. Qomi, *Rev. Roum. Chim*., **66**, 493–507 (2021).
26. D. Ghemati, D. Aliouche, *J. Appl. Spectrosc.*, **81**, 257–263 (2014).
27. R. Masoudi, H. Moghimi, E. Azin, R. A. Taheri, *Artif. Cells, Nanomed., Biotechnol.,* **46**, S1092–S1101 (2018).
28. N. Lamaiphan, C. Sakaew, P. Sricharoen, P. Nuengmatcha, S. Chanthai, N. Limchoowong, *J. Korean Ceram. Soc*., **58**, 314–329 (2021).
29. M. Abniki, A. Moghimi, *Micro & Nano Letters*, **16**, 455–462 (2021).